Proceedings of the 4th WSEAS/IASME Int. Conf. on System Science and Simulation in Engineering, Tenerife, Spain, December 16-18, 2005 (pp106-113)

Mechanical characterization of a viscoelastic plastic granular material sensitive to hydrostatic pressure

[a] M. GRATTON, [a]V.D. LE, [a]A. FRACHON[a], [a]M. CALIEZ, [b]D. PICART
[a] Laboratoire de Mécanique et Rhéologie, Université F-RABELAIS TOURS,
Ecole d'Ingénieurs du Val de Loire, Rue de la chocolaterie - BP3410 - 41034 Blois cedex
[b] C.E.A. Le Ripault, BP16 – 37260 Monts
FRANCE
http://www.polytech.univ-tours.fr/lmr,
http://www.cea.fr

Abstract: This paper deals with the characterization of the static mechanical behaviour of an energetic material. Due to the constituents (crystals and a polymeric binder), the behaviour is complex. Therefore, a complete experimental protocol and a model have been developed. The behaviour is described using a general Maxwell model in which all the branches are affected by isotropic damage. The first branch takes into account an elastic-plastic behaviour. The yield stress evolution is described by a parabolic criterion and by an isotropic hardening law. The plastic flow rule is nonassociated. The other branches are viscoelastic. A genetic algorithm has been used to optimise the parameters. At last, comparisons between the model and the experiments are proposed.

Key-Words: Energetic material, Parabolic plastic criterion, Genetic algorithm, DMA, Viscoelasticity, Isotropic damage.

1 Introduction

The material is made of organic and energetic crystals mixed with a few percentage of a polymeric binder. After an isostatic compaction forming process, the material has a small porosity of a few percent. Samples can be machined in several geometric shapes, which are more than ten times the length of the material heterogeneity.

In order to survey the possible influence of aging on the behaviour of this material, an accurate determination of the mechanical properties has to be done. Unfortunately, this material being available in small amounts, the characterization must be made using a reduced number of standard tests. An unusual experimental procedure is proposed in this paper for this kind of material. When monotonic loading paths were used to determine for example the influence of the strain rate, each sample is submitted to complex loading paths including relaxation, recovery and cyclic conditions.
The temperature-dependence is out of the scope of this paper, therefore all the tests reported here have been performed at room temperature.
The observation of loading-unloading diagram on figure 1 shows some of the main features of the material, and entails specific arrangements for the mechanical tests. 1) Hydrostatic pressure sensitivity: this influence is related to the material plastic behaviour. To take it into account, an initial hydrostatic compression loading path (0 MPa, 5 MPa and 10 MPa) is made before the run of an uniaxial compression load. 2) Viscosity: different strain rates ($5.10^{-6}s^{-1}$ to $10^{-3}s^{-1}$) have been used to observe such effect. The parameters of the viscoelastic part of the behaviour have been determined using a DMA apparatus (Dynamic Mechanical Analysis). 3) The plastic strains are determined using relaxation and recovery delays. 4) Initial elastic behaviour: standard tests made in various material directions show an initial isotropic behaviour. 5) Damaging: systematic cyclic loading-unloading programs have been performed. 6) Dispersion: to ensure a minimum statistical validity, each loading program is repeated five times.
The whole process of characterization is described in the second part of this paper.

This experimental process provides a numerical data set from which the material characterization can be drawn. The main models available in the literature ([1-3]) for this kind of material have been developed for transient dynamic behaviour and are not adapted for a quasi-static study. For example, the influence of the pressure is omitted, even as the difference of behaviour observed in tension and compression loading paths.
The Maxwell model we have chosen is close to the constitutive law proposed in [2] (fig. 2). Several damageable viscoelastic branches and one damageable elastoplastic branch are used. The main difference with Bennett and co-workers model is about the arrangement of the branches, which evolutions are here related to the strain coming from the global equilibrium state.
The determination of the plastic (resp. viscoelastic) behaviour is described in the third (resp. fourth) part of this paper. In particular, a genetic algorithm has been used to optimize the determination of the viscoelastic parameters. An extensive presentation is proposed in the

part 4 of this paper. The part 5 deals with the damage rule and the proposed failure threshold. It could be noted that the characterization of the plasticity, the damage and the viscosity are uncoupled. The damage rule determined from the plastic analysis is assumed to affect also the viscoelasticity.

Lastly, some comparisons are presented between the model response and the available experimental data.

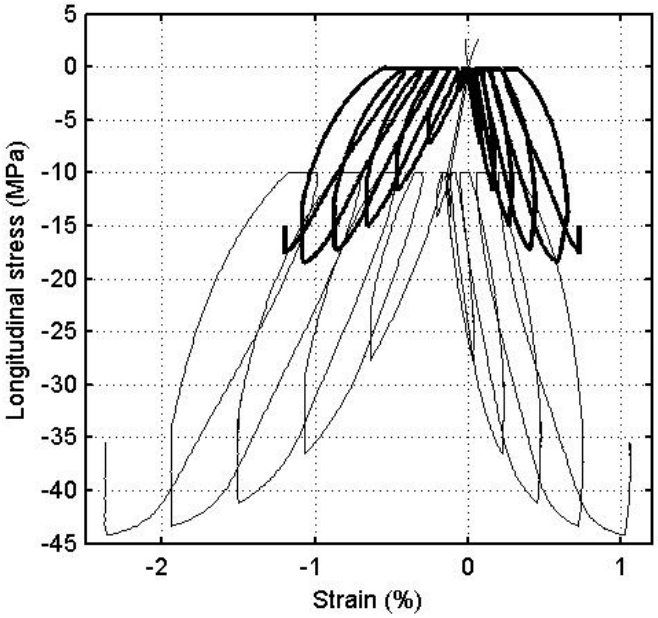

Fig. 1: Material behaviour in tension (positive stress), compression (thick line) and for a triaxial compression test at 10 MPa (thin line).

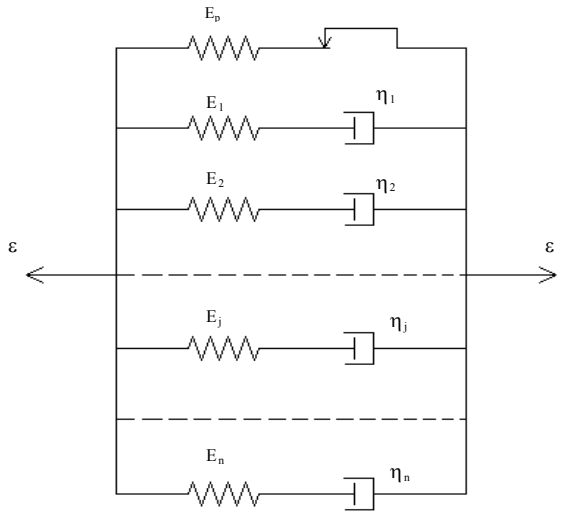

Fig. 2: Rheologic diagram of the viscoelastic plastic damageable model. Damage is applied to the E_i.

2 Test procedure

Cylindrical samples of 10 mm radius and 20 mm height are used for compression tests, and halters of 150 mm length with a rectangular cross section of 10 mm side for tension tests. A 100 kN machine is equipped to perform, control and record strains and stress.

The samples are equipped with opposite pairs of strain gages whose outputs are averaged (after estimation of the heterogeneity of the strain) to provide the longitudinal and lateral strains. Stress is obtained from the longitudinal force applied by the machine. The triaxial compression experiments have been made using a tool usually used for geomaterial characterization (hermetic cell, pressure controller and water). The tension experiments are realized without a hydrostatic pressure.

The loading program is illustrated on figure 3. The first stage (when this one exist) is a hydrostatic loading phase (segment OA_1). Then, five or six uniaxial loading-relaxation-unloading-recovery cycles are done (loop $A_iB_iC_iD_iA_{i+1}$). The test is driven by one of the two longitudinal gages. Relaxation times have been defined to guarantee an almost complete relaxation of viscous stresses. It has been established that a 30 mn (resp. 50 mn) time for the relaxation (resp. recovery) phases are adequate.

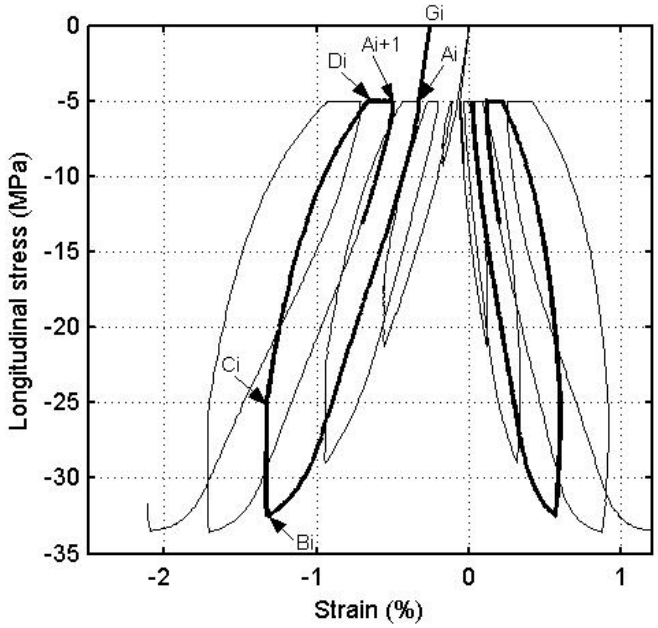

Fig. 3: Cyclic compression under 5 MPa of pressure: stress versus longitudinal and lateral strains.

Using the recorded measurements, the following data are picked up. At point C_i, the strains and the stress define a point of the current yield surface of the plastic branch (the viscoelastic branches are relaxed). The slope E_{ep} of the line C_iA_{i+1} defines the current elastic modulus of this branch. The segment $A_{i+1}G_i$, whose slope is assumed to be $E_{ep}/(1-2\nu)$, gives the current plastic strain. If a constant bulk modulus is assumed during the test, then $\varepsilon_p = \overline{OG_i} = \overline{A_1A_{i+1}}$.

Some DMA experiments have been realized in compression using samples of 50 mm long, and a cross section of 4x4 mm^2. A small initial preload of 10 μm and for a very small strain amplitude of 5 μm are used to stay in the viscoelastic domain. The range of frequencies going from 0.004 to 40 Hz, the strain rate ranges from 2.10^{-6} s^{-1} to 2.10^{-2} s^{-1}.

3 Elastoplasticity

The macroscopic stress tensor $\underline{\underline{\sigma}}$ is defined as the sum of the stress of each branch:

$$\underline{\underline{\sigma}} = \underline{\underline{\sigma}}_{ep} + \sum_{j=1}^{n} \underline{\underline{\sigma}}_{j} ,$$

where the subscript "ep" (resp. "j") denoted the elastoplastic branch (resp. the j^{th} viscoelastic branch). An additive decomposition is assumed for the strain of each branch between an elastic part (superscript "e") and a plastic (resp. viscous) part (superscript "p" or "v"):

$$\underline{\underline{\varepsilon}} = \underline{\underline{\varepsilon}}_{ep}^{e} + \underline{\underline{\varepsilon}}_{ep}^{p} \text{ elasto-plastic branch,}$$

$$\underline{\underline{\varepsilon}} = \underline{\underline{\varepsilon}}_{j}^{e} + \underline{\underline{\varepsilon}}_{j}^{v} \qquad \text{visco-elastic branches .}$$

3.1 Elasticity

The elastic part is supposed linear damageable and given by the following equation:

$$\underline{\underline{\sigma}}_{ep} = (1-d)\mathbf{E} : \underline{\underline{\varepsilon}}_{ep}^{e} ,$$

where **E** is the elastic tensor of the virgin material and *d* a damage parameter (see below). To identify the elastic mechanism, we need to isolate the elastoplastic behaviour (in particular to be sure that the viscous stresses are relaxed). To this end, the end of the relaxation phase is used in conjunction with the end of the recovery part of the cyclic tests. These points are used to determine the elastic modulus and its evolution. For the Poisson's ratio, the longitudinal and transversal strains measurements are used. Then, a value of 0.3 is obtained for the Poisson's ratio when an initial Young's modulus of 3000 MPa is determined at room temperature. The previous Poisson's ratio is also used for the viscoelastic branches.

3.2 Yield criterion

A review of the main criteria used to describe isotropic plasticity is presented in [4]. A criterion has been developed at Cambridge University in view of soil modeling and is famous to-day as the "Cam-clay" model [5]. Numerous adaptations of this model were then developed for various applications [6-8]. As the forming process of the material is an isostatic compaction up to a pressure of 200 MPa (which amplitude will never be reached in quasi-static applications), the criteria is supposed open on the hydrostatic negative axis. Open threshold are usually derived from Mohr-Coulomb, Mises-Schleicher [9], Drucker-Prager [10] and more recently Hoek-Brown formulations [11]. An unified model is proposed by Aubertin and co. [4] in order to reproduce all the kinds of criterion (elliptic, parabolic, hyperbolic). Lastly, Raghava and co. [12] applied the Mises-Schlecher's threshold to polymers. The evolution of this criterion is described by two hardening variables, associated to tensile and compression response.

Due to a lack of data about the nature of the hardening mechanisms, an isotropic hardening parameter, denoted *k*, is introduced in the model. The short softening behaviour which is observed during the compression tests (tensile experiments have shown a brittle failure process) is ignored. Then, a saturation of the hardening mechanism at the maximum stress is taken into account in the model.

A nonlinear plasticity criterion reproduces the evolution of the yield stress (fig. 4). The following relation is used:

$$f(Q,P,k) = \sigma_{eq} - k = 0 \text{ , with } \sigma_{eq} = \sqrt{Q^2 + b(k)P}$$

where $Q = \sqrt{(1/3)\ \underline{\underline{\sigma}}^{d} : \underline{\underline{\sigma}}^{d}}$ is the octahedric stress, $\underline{\underline{\sigma}}^{d}$ the deviatoric stress, P the pressure and *b*, a function of the hardening parameter, defined by: $b(k) = \dfrac{k^2}{X(k)}$.

The set of yield curves is completely defined as soon as the function *X(k)* and the hardening law are defined.

The following guidelines help for the determination of the function *X(k)*. First, it is assumed that the yield curves do not cross themselves in the *P*-*Q* plane, each one being embedded in those of higher levels, all of them being embedded in the extreme curve. This is a necessary - but not sufficient - condition for the phenomenon to be governed by a unique state variable which is the isotropic strain-hardening parameter.

Elementary algebra shows that the following relation satisfies the previous assumption:

$$X(k) = X_0 + (X_m - X_0)\frac{k - k_0}{k_m - k_0} ,$$

where k_0, X_0, k_m and X_m are four material parameters.

Then, the two parameters X_m and k_m are determined using the ultimate yield stress curve relating the maximum stress states in the *P*-*Q* plane. The following values are obtained: X_0=1.5 MPa, X_m=1.62 MPa, k_o=1 MPa and k_m=3.45 MPa.

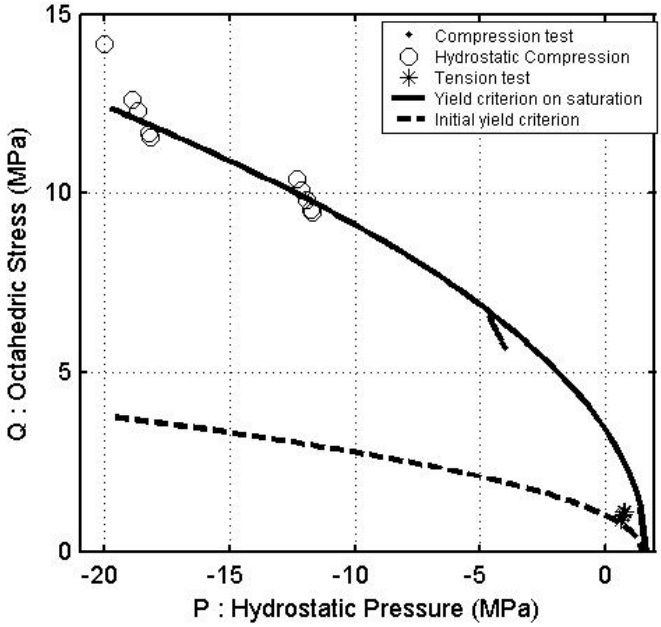

Fig. 4: Yield criterion joining the maximum relaxed stresses (saturation).

The hardening parameter k has to be related to an effective plastic strain variable, denoted p. In order to obtain an unique curve $k(p)$ for all the available experimental data available, p is defined as the cumulated deviatoric plastic strain (fig. 5). For the hardening law, the following hyperbolic relation is used to interpolate the data:

$$k = k_0 + (k_m - k_0)\left(1 - \frac{1}{1 + c_1\, p + c_2\, p^2}\right),$$

where c_1 and c_2 are two parameters. The determination of the parameters gives c_1=450 and c_2=1.4 10^5.

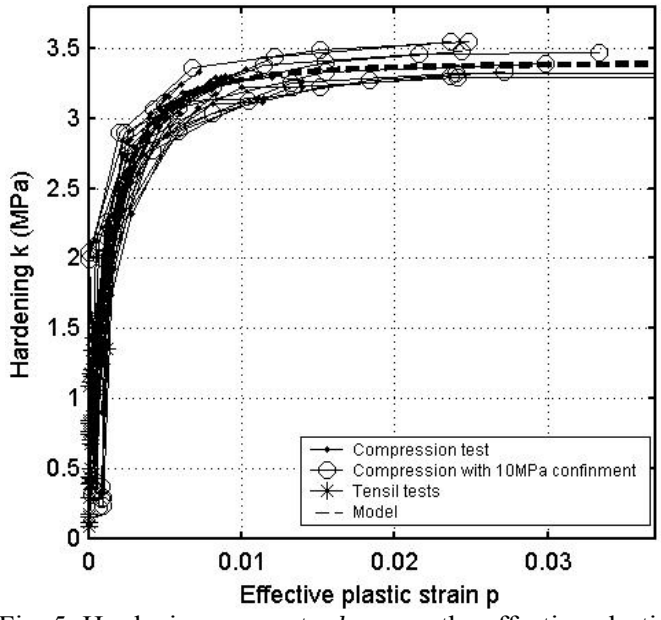

Fig. 5: Hardening parameter k versus the effective plastic strain p. The saturation of the hardening is observed.

3.3 Flow rule

The flow direction is determined using the ratio between volumic and deviatoric effective plastic strain rates. This ratio, usually called "dilatancy" and denoted here β, is given by the following relation:

$$\beta = \frac{\dot{\varepsilon}_{ep}^{pV}}{\dot{\varepsilon}_{ep}^{pD}},$$

with $\dot{\varepsilon}_{ep}^{pV} = \mathrm{tr}(\dot{\underline{\underline{\varepsilon}}}_{ep}^{p})$ and $\dot{\varepsilon}_{ep}^{pD} = \sqrt{3\, \dot{\underline{\underline{\varepsilon}}}_{ep}^{pD} : \dot{\underline{\underline{\varepsilon}}}_{ep}^{pD}}$, $\dot{\underline{\underline{\varepsilon}}}_{ep}^{pD}$ being the deviatoric plastic strain rates.

The flow rule expression is then:

$$\dot{\underline{\underline{\varepsilon}}}_{ep}^{p} = \dot{\lambda}\left(\frac{\underline{\underline{\sigma}}_{ep}^{d}}{3Q} + \frac{\beta}{3}\underline{\underline{I}}\right).\sqrt{\frac{3}{(1+\beta^2)}},$$

$\dot{\lambda}$ being the plastic multiplier and the plastic flow direction being normalized.

The dilatancy β measured during the experiments is plotted on the figure 6. A linear fit allows to determine a constant value for β(0.3). As a result, a nonassociated plastic law is justified.

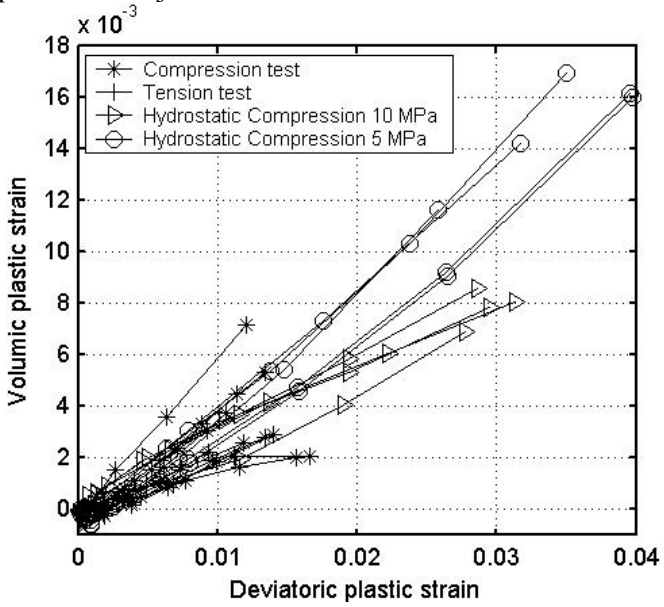

Fig. 6: Effective volumic plastic strain versus effective deviatoric plastic strain for whole tests. The slope of the mean curve determine the dilatancy parameter β.

4 Viscoelasticity

The DMA experiments are used to make a first identification of the linear viscoelastic parameters. The stress response to an unit sinusoidal strain solicitation for this kind of model can be break up in an in-phase part (related to the storage modulus E_{real}) and a out of phase part (related to the loss modulus E_{imag}). The relations between these two quantities and the Young's modulus

and the viscosity parameters are given by:

$$E_{real} = E_{ep} + \sum_{i=1}^{n} E_i \frac{(\tau_i.\omega)^2}{1+(\tau_i.\omega)^2}$$

$$E_{imag} = \sum_{i=1}^{n} E_i \frac{(\tau_i.\omega)}{1+(\tau_i.\omega)^2}$$

with $\tau_i = \frac{\eta_i}{E_i}$, where η_i is the viscosity parameter and ω is related to the pulsation.

In order to limit the number of parameters (here n=10) for a more accurate determination, the following relations are proposed:

$$\eta_i = 10^{\left(A_1 \frac{i-1}{n-1} + A_2\right)}$$

$$E_i = A_3 + A_4\left(e^{\left(A_5 \frac{i-1}{n-1}\right)} - 1\right)$$

Then, the number of unknowns decreases to five (A_1 to A_5). These relations allow reproducing at the same time the real and the imaginary modulus. A first determination of the A_i has been obtained using DMA measurements: A_1 = 5, A_2 = 1.3, A_3 = 180, A_4 = 10.8 and A_5 = 3.3. For these parameters, the maximum (resp. minimum) relaxation time is 4318 s (resp. 0.111 s).

4.1 Genetic algorithm

The previous set of parameters is used here to determine the bounds of each parameter. We are here in the case of a combinatory optimisation problem where a large number of solutions could be suitable. We have chosen to perform an inverse identification of the viscoelasticity parameters directly from the experimental tests. Classical optimisation methods, like conjugated gradient, have been dismissed because of the possible large number of solutions. Then, a genetic algorithm [13] has been used in this study.

Genetic algorithms are based on the Darwinian principle of "survival to the fittest". An initial population of a given size is created from a random selection of parameters values. Each parameter set represents individual chromosomes. Each individual is assigned of a fitness based on how well each individual chromosome allows it to perform in its environment. The algorithm produces new generations by applying three evolution operators: selection, crossover and mutation. For each generation, the fit individuals survive and the weak die. Evolution operators create new individuals (children) from two selected parents, and these children replace the weak individuals for the next generation. Successive generations are created until very fit individuals are obtained. This algorithm offers the advantage of exploring all the solutions space to find a global optimum of an optimization problem. A sensitivity analysis of the parameters is not required

4.2 Objective function

The objective function is a direct measure of the quality of a solution. The goal is here to minimize the gap between the experimental strain-stress curves and the corresponding simulated curves. Due to different times of recording during the experiments, we propose a fitness function that represents the spatial gap, weighted by the segment length L_i between two consecutive data, in the stress-strain space, i.e.:

$$Obj = \sum_{i=1}^{nb\,exp\,pts} \frac{\sqrt{\left(\sigma_i^e - \sigma_i^s\right)^2 + \left(\frac{1}{2}E\right)^2 \left(\varepsilon_i^e - \varepsilon_i^s\right)^2}.\,L_i}{\sum_{i=1}^{nb\,exp\,pts} L_i}$$

where superscripts "s" and "e" respectively denote simulations and experiments.

4.3 Selection

The selection process is based on the objective function value. Individuals are ranked in a increasing order of their objective values and have a position called *Pos*. The following relation then assigns a fitness function to each individual:

$$f(Pos) = 2 - SP + 2\frac{(SP-1)(Pos-1)}{N_{ind}-1}$$

where N_{ind} is the total number of individuals and *SP* is the selection pressure, i.e. the maximal value of the fitness function assigned to the best individual. The weakest individual has a fitness value of 0. We apply here a proportional selection technique. Each individual has then a probability to be selected which is given by:

$$Pi = \frac{fitness(i)}{\sum_{j=1}^{Nind} fitness(j)}$$

An individual with a nul fitness value has a nul probability of selection. The best one has the larger probability.

4.4 Crossover and mutation

After selection, two evolution operators are applied on individuals: crossover and mutation. Two probabilities P_c and P_m are respectively assigned to these operators. A number is randomly created between 0 and 1 for each individuals. If this number is lower than P_c, this individual becomes a parent, which is going to produce two children with another parent. The crossover consists to exchange the chromosome (which is a parameter value) between two parents. The resulting individuals

become two children. The choice of the chromosome results of a randomly generated mask.
The second operator is the mutation. For each chromosome constituting an individual, a random number is generated between 0 and 1. If this number is lower than P_m, a random number is added to the chromosome. This number depends on the minimal and maximal proposed values.

4.5 Results

The simulation use the data corresponding at the end of load, the end of relaxation, the end of discharge and the end of recovery. From the values of the longitudinal strain and time in these points, the strain rate is rebuilt, constant by piece. The strain increment is then given from the strain rate and the step of time of the program.
Let us note that only the longitudinal strain is imposed. The longitudinal stress and the transverse strain are recomputed from the response of the model.
P_c and P_m have been respectively set to 0.8 and 0.05, which are common values for this kind of optimization problem. 60 generations constituted of 500 individuals have been performed and leads to the optimized values of the A_i parameters: A_1=3.98, A_2=1.64, A_3=160.31, A_4=16.15 and A_5=1.21.

5 Damage and fracture criterion

5.1 Isotropic damage

Assuming an isotropic damage, experimental data shows that the phenomenon regularly increases with the highest positive principal strain (figure 7). This observation indicates that the most probable damaging mechanism is the result of the development of internal micro-defects (cavities, cracks) with tension [14-19]. A damaging factor d is classically defined as:

$$d = \frac{E_0 - E}{E_0}$$

where E_o and E are the initial and current Young's modulus. A constant Poisson's ratio is assumed here.
An hyperbolic relation is used to reproduce an average evolution of the damaging factor, providing that its value is bounded to 1. Experimental values of d immediately result from the measurements of E and the following relation:

$$d = \left(d_1 \cdot \underbrace{\sup}_{\text{time}} \left\langle \underbrace{\max}_{I=1 \text{ to } 3} (\varepsilon_I) \right\rangle_+ + d_2 \right) \cdot \left(1 - \frac{1}{1 + d_3 \underbrace{\sup}_{\text{time}} \left\langle \underbrace{\max}_{I=1 \text{ to } 3} \varepsilon_I \right\rangle_+} \right)$$

where d_1, d_2 and d_3 are three parameters. The subscript "+" means "the positive part of the quantity".
The damage rule is reported in the figure 7. One can see that the model response is identified using the compression and tension measurements. The hydrostatic data are not taken into account because the pressure stops an eventually growth of the microcavities. The identified values are: d_1 = 3, d_2 = 1 and d_3 = 100.

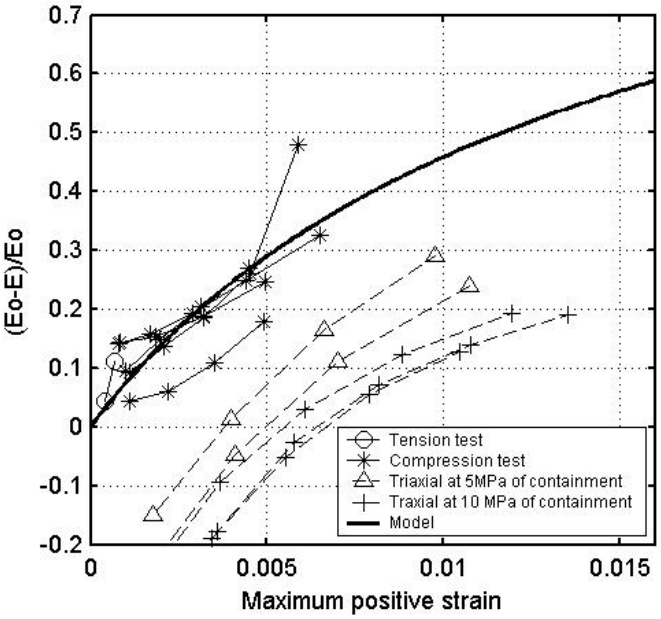

Fig. 7 : Damage versus the maximum positive strain.

5.2 Fracture criterion

A threshold based on the damage level is not able to describe the ultimate data in tension and compression. So, two thresholds have been proposed. The first one describe the failure under tension loading path (the maximum effective stress is used) and the second one is based on the maximum positive strain (fig. 8).

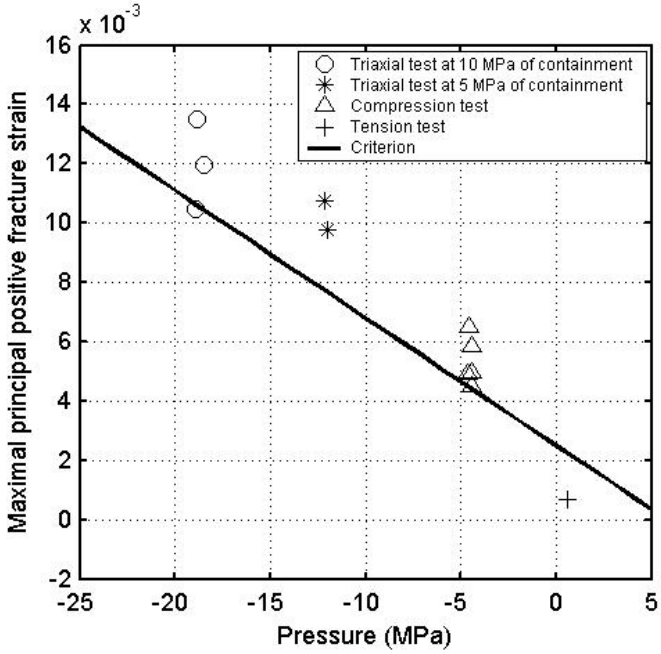

Fig. 8: Maximum positive strain versus the mean pressure. For the compression state of stress, a linear threshold can be used to determine the failure.

6 Model versus experiments

The constitutive law has been implemented in the finite element code Abaqus/standard. The model is compared to experimental data with unloading cycles to access to the plasticity level and the damage level. Those seem quite well reproduced even if the transversal model response does not present enough damage in compression (fig. 9). This observation can be associated to an anisotropic damage (which has been neglected here).

The plasticity branch reproduces very well the difference between traction and compression response (fig. 9-10).

The rate effect is also quite well reproduced on the two compression tests even if the unloading curves do not present the same nonlinearity (fig. 9 and 12). In the same manner, the viscous effects in the triaxial test with 10 MPa of confinement pressure (fig. 11) is underestimated. Certainly, those phenomenons are associated to an internal friction in the material.

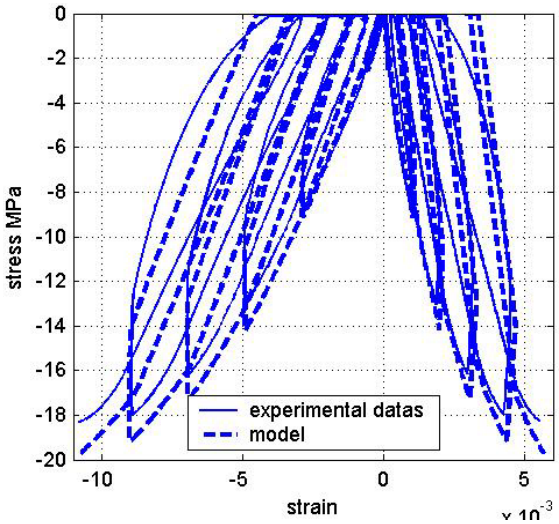

Fig. 9: Model versus experiment for the compression test at 3.10^{-6} sec^{-1}.

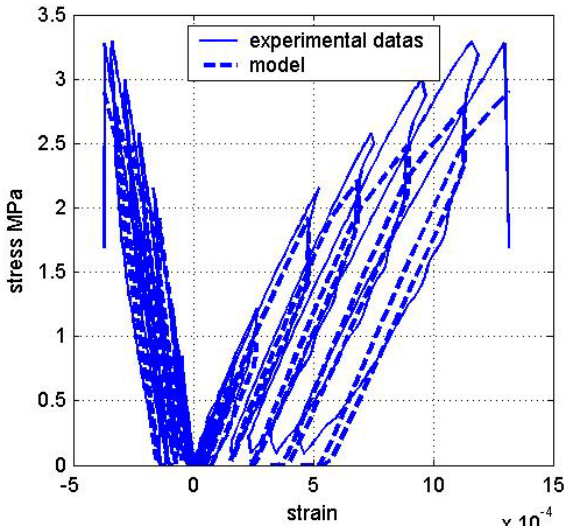

Fig. 10: Model versus experiment for the tensile test (3.10^{-5} sec^{-1}).

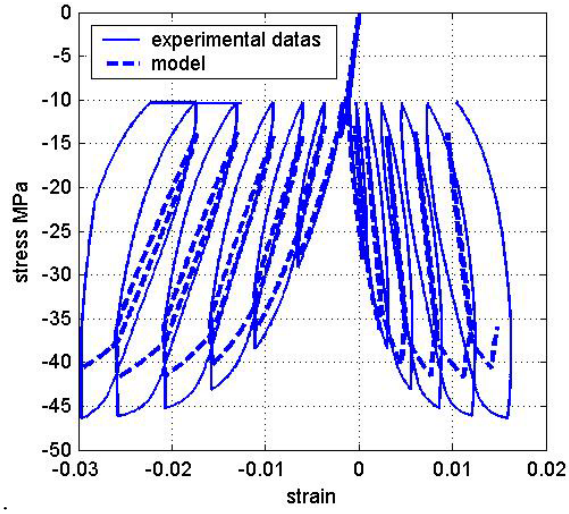

Fig. 11: Model versus experiment for the hydrostatic compression test (3.10^{-5} sec^{-1}).

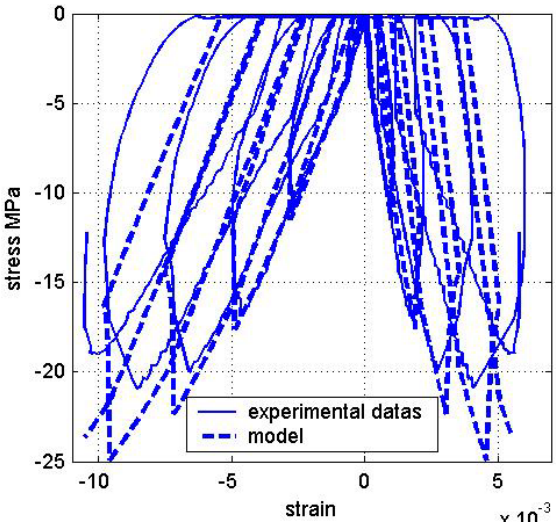

Fig. 12: Model versus experiment for the compression test ($1.5\ 10^{-3}$ sec^{-1}).

The implementation of the constitutive law in the finite element code has allowed to compare simulations to more complex experimental configurations as three-point bend tests and Brazilian experiments. For the sake of simplicity, these results are not reported here but are going to be detailed in a next paper.

7 Conclusion

An experimental procedure has been carried out to characterize a complex material behaviour. A multibranch viscoelastic plastic and damageable model and the corresponding identification procedure have been developed. A genetic algorithm optimisation has allowed to find accurately some of the parameters. This model has been implemented in the finite elements software Abaqus using an user subroutine UMAT. The

comparisons between simulations and experiments show a good agreement.
Our future works are now devoted to the improvement of the damage rule and of the failure threshold. Lastly, the anisotropy observed during the experiments has to be introduced in the model.

Acknowledgement:
The authors address a special thinks to J.L. Brigolle for its contribution to this study, especially for the realization of the experiments.

References:
[1] F.L. Addessio, J.N. Johnson, A constitutive model for the dynamic response of brittle materials, J. Appl. Phys., Vol. 67, 1990, pp 3275-3286.
[2] J.G. Bennett, K.S. Haberman, J.N. Johnson, B.W. Asay, B.F. Henson, A constitutive model for the non-schock ignition and mechanical response on high explosives, *J. Mech. Phys. Solids*, Vol. 46-12, 1998, pp. 2303-2322.
[3] R.M. Hackett, J.G. Bennett, An implicit finite element material model for energetic particulate composite materials, *Int. J. Numer. Meth. Engng*, Vol. 49, 2000, pp. 1191-1209.
[4] M. Aubertin, L. Li, A porosity-dependant inelastic criterion for engineering materials, *Int. Jour. of Plast.*, Vol. 20, 2004, pp. 2179-2208.
[5] J.H. Prevost, R. Popescu, Constitutive Relations for Soil Materials, *Electronic Journal of Geotechnical Engineering*, First Issue, 1996.
[6] O. Coussy, *Mécanique des Milieux Poreux*. Editions Technip, 1991.
[7] A. Bouchou, M. Gratton, C. Gontier, Un modèle phénoménologique pour l'étude de la compression d'une mousse phénolique, *Acts of the fifth* national *conference in structures computation*, Giens, Vol I, 2001, pp. 393-400.
[8] P.Y. Hicher, J-F. Shao, Elastoplasticité des sols et des roches - Modèles de comportement des sols et des roches - 1, Hermès Science Publications, 2002.
[9] F. Schleicher, Z. Angew, Math. Mech., 6:199, 1926.
[10] D.C. Drucker, A.M. Asce, R.E. Gibson, & D.J. Henkel, Soil Mechanics and Work-Harding theories of plasticity, Transactions American Society of Civil Engineers, Vol. 122, 1957.
[11] X.D. Pan, J.A. Hudson, A simplified three dimensional Hoek-Brown yield criterion, *Rock Mechanics and Power Plants, M. Romana* (ed.), Rotterdam: Balkema, 1988, pp. 95-103.
[12] R. Raghava, R.M. Caddekk, G.S.Y. Yeh, The macroscopic yield behaviour of polymers, *J. Material Science*, Vol.8, 1973, pp. 225-232.
[13] D.E. Goldberg, Genetic algorithms in search, Optimization and Machine Learning, Addison Wesley Publishing Company, 1989.
[14] J. Mazars, Mechanical damage and fracture of concrete structure, Proc. I.C.F. 5, Cannes, France, 1981, pp. 1499-1506.
[15] A. Dragon, D. Halm, Th. Désoyer, Anisotropic damage in quasi-brittle solids: modelling, computational issues and applications, Comput. Methods Appl. Mech. Engrg., 183, 2000, pp. 331-352.
[16] D. Halm, A. Dragon, An anisotropic model of damage and frictional sliding for brittle materials, Eur. J. Mech., A/Solids, Vol.17, No. 3, 1998, pp. 439-460.
[17] J. Mazars, Application de la mécanique de l'endommagement au comportement non linéaire et à la rupture du béton de structure, Université Pièrre et Marie Curie – Paris 6, 1984.
[18] J. Mazars, A description of micro- and macroscale damage of concrete structures, Engineering Fracture Mechanics, Vol. 25, No. 5/6, 1986, pp. 729-737.
[19] J. Mazars, F. Ragueneau, G. Pijaudier-Cabot, Continuum damage modelling for concrete structures in dynamic situations, Continuum Damage Mechanics of Materials and Structures, O. Allix and F. Hild (Editors), Elsevier Science Ltd., 2002.